Self-Calibration Using the Finite Element Approach

Raidh A. Halim Munjy
Civil & Surveying Engineering Department, California State University – Fresno, Fresno, CA 93740

ABSTRACT: Theoretical and practical aspects of the finite element approach in self-calibration developed by the author have been investigated in detail. An experimental verification of the proposed technique has been carried out. The experimental results support the conclusion that the reported technique gives a good representation of the systematic errors in photogrammetry.

INTRODUCTION

SINCE ABOUT 1956 the finite element method has developed enormously. It began as a numerical method of stress analysis and is still most widely used for this purpose (Cook, 1974). In addition, it has become popular in many other areas including heat conduction, seepage flow, fluid dynamics, acoustics, electric and magnetic fields, and recently in digital terrain modeling (Ebner *et al.*, 1978, 1980, 1981).

Photogrammetry can be described as a non-contact measuring technique which extracts reliable geometric measurements from imagery records. Generally, this measuring technique is categorized into two fields: analog and analytical photogrammetry. The last two decades have witnessed a tremendous growth for the analytical approach due to developments in high speed digital computer technology, and the growing importance of non-conventional photogrammetry.

In the analytical approach, systematic errors in photogrammetry are compensated for by mathematical functions (e.g., orthogonal polynomials). In many cases these mathematical functions yield no insight into the physical or mechanical source of the errors. It will be shown that the finite element approach can play an important role in modeling these errors and in increasing photogrammetric accuracy.

In photogrammetry, the finite element method can be used to study and investigate many problems such as camera calibration, film shrinkage, camera stability, flatness of film during exposure, mono- and stereo-comparator calibration, distortions in X-ray photogrammetry, and in underwater photogrammetry. It can also be used to correct distortions in satellite imagery. The finite element approach in analytical self-calibration forms the topic of this paper.

A search of the current literature (see, for example, Brown (1971), Brown (1972), Kenefick *et al.* (1972), Ebner (1976), and Fraser (1979)) reveals that the present state-of-the-art in analytical self-calibration is basically as follows:

> Analytical approaches to camera calibration have a common starting point: compensation of systematic image coordinate errors by analytical models incorporated into the photogrammetric projective equation. The parameters defining systematic errors are then recovered simultaneously with the projective parameters (position, orientation, focal length, principal point) in a least-squares adjustment leading to the minimization of the quadratic form of the residuals of measured quantities.

Most reported analytic functions representing film shrinkage, film flatness, and radial lens distortion are assumed to be valid throughout the image plane. A logical extension of this theory is to divide the image plane domain into subdomains or finite elements and then to prescribe a mathematical model for systematic errors over the image plane domain in a piecewise fashion, element by element, thus eliminating the assumption of symmetry.

THE BASIC IDEAS OF THE FINITE ELEMENT METHOD

The finite element method can be described in a few words. Suppose that in the problem to be solved it is required to find a function v which minimizes a given expression. This minimizing property leads to a differential equation for v (the Euler Equation), but normally an exact solution is impossible and some approximation is necessary. A trial solution is considered in which v is approximated by a solution v_m of linear form

$$v_m = \sum_{r=1}^{M} C_r P_r \qquad (1)$$

where P_r are linearly independent selected functions existing over the domain and its boundary and C_r are unknown parameters to be determined, not by a differential equation, but by a system of M discrete

PHOTOGRAMMETRIC ENGINEERING AND REMOTE SENSING, Vol. 52, No. 3, March 1986, pp. 411–418.

0099-1112/86/5203-411$02.25/0

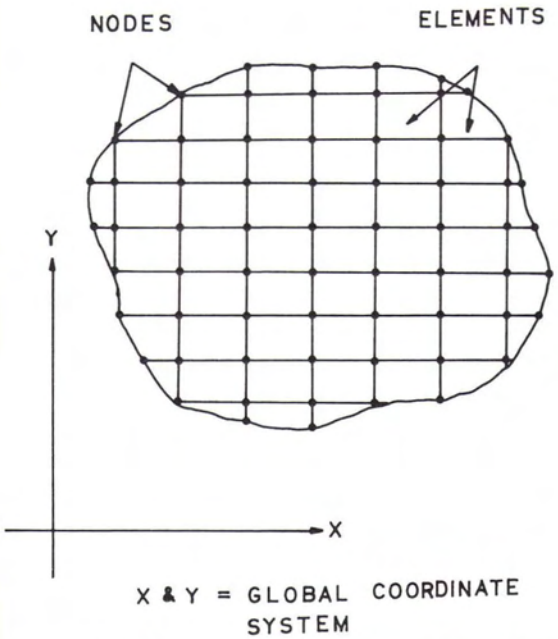

FIG. 1. Subdivision into finite elements of arbitrary continuum.

algebraic equations which the computer can handle (Strang *et al.*, 1973).

The finite element process as described so far is identical to the Rayleigh-Ritz procedure. The difference is only the manner in which the function v is prescribed. In the Ritz process, the traditionally used function v is usually given by an expression valid throughout the whole region, thus leading to simultaneous equations in which no banding occurs and the coefficient matrix is full. In the finite element process this specification is usually piecewise, each nodal parameter influencing only adjacent elements, and thus a sparse and usually banded matrix of coefficients is found (Zienkiewicz, 1977).

Thus, the key features of the finite element concept according to Norrie *et al.* (1973) are

- The domain is divided into subdomains or finite elements, usually of the same form (Figure 1); and
- The trial solution is prescribed (functionally) over the domain in a piecewise fashion, element by element.

The accuracy of the finite element method can be increased, if that is necessary, but not by the classical Ritz method of including more and more complex trial functions. Instead, the same functions are retained, and the subdivision is refined.

ELEMENTS AND THEIR SHAPE FUNCTIONS

The discretization principle in the finite element method involves the division of a continuum (Figure 1) into an equivalent system of smaller continua. In one-dimensional problems, the continuum is divided into line elements, linear or curved. Triangles and quadrilaterals are common shapes used for two-dimensional problems. In three-dimensional analyses, the common elements used are tetrahedra and hexahedra. In this paper, the emphasis will be on the two-dimensional problems.

In two-dimensional analysis the simplest element shapes are obviously a triangle and quadrilateral defined by three or four nodes, respectively. Triangles are obviously better at approximating a curved boundary, but there are advantages to quadrilaterals (especially to rectangles) in the interior, as there are fewer of them, and higher order functions can be very easily used (Strang *et al.*, 1973).

TRIANGULAR ELEMENTS

The most basic and simplest of all trial functions is

$$v(x,y) = a_1 + a_2 x + a_3 y \qquad (2)$$

This function is linear inside each triangle and continuous across each edge. Thus, the graph $v(x,y)$ is a surface made up of flat triangular pieces, joined along the edges. This is an obvious generalization of broken-line functions in one dimension.

The three coefficients of Equation 2 are uniquely determined by the values of the function v at the three nodes. This means that the function can be conveniently described by giving its nodal values. Furthermore, along any edge, it reduces to a linear function of one variable, and this function is obviously determined by its values at the two end points of the edge. The value of v at the third vertex has no effect on the function along this edge, regardless of whether this vertex belongs to the triangle on one side or the other. Therefore, the continuity across the edge is assured by continuity at the vertices.

The approximation function v in Equation 2 is of class C^o. An approximation function is considered of class k if it has continuous derivatives across the element boundaries of order k (Strang, et al., 1973).

There are other trial functions beside the linear function described in the literature (see, for example, Zienkiewicz (1977), Strang *et al.* (1973)), but such trial functions will need more than three nodes to define the function over the triangle.

Equation 2 can also be written in terms of the values of the function at the nodes

$$v = l_1 v_i + l_2 v_j + l_3 v_k \qquad (3)$$

where l_1, l_2, l_3 are the triangular coordinates (Cook, 1974).

RECTANGULAR ELEMENTS

Rectangles are a special case of a quadrilateral. However, a quadrilateral can be transformed to a rectangular shape by using a bilinear coordinate transformation (Ergatoudis, 1968). Linear functions

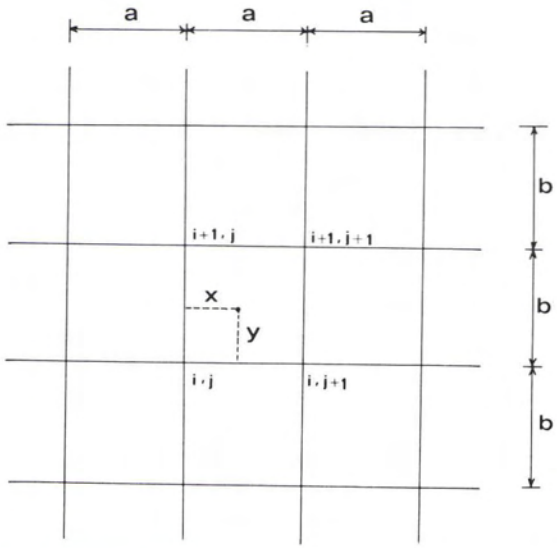

FIG.2. Rectangular grid mesh.

in rectangular elements will be discontinuous across the boundaries. So the simplest construction, in analogy with the linear element for triangles, is based on a piecewise bilinear function with class C^o in each rectangle; that is,

$$v(x,y) = a_1 + a_2 x + a_3 y + a_4 xy \qquad (4)$$

where a_1, a_2, a_3, a_4 are coefficients determined by the value of the function at the vertices of the rectangle.

It is important to notice that, for arbitrary quadrilaterals, these piecewise bilinear functions would not be continuous from one element to the next. Suppose that two quadrilaterals are joined by a line $y = mx + b$. Then along that edge, the bilinear function reduces to a quadratic; it is linear only if the edge is horizontal or vertical. A quadratic cannot be determined from the two nodal values at the end points of the edge, and in fact the other nodes do affect the value of v. Therefore, bilinear elements may be used only on rectangles (Strang *et al.*, 1973).

Equation 4 can be written using the value of the function at the nodes. For a rectangular grid mesh as in Figure 2, the bilinear equation will be

$$(5) v = [1 - x/a,\ x/a] \begin{bmatrix} v_{i,j} & v_{i+1,j} \\ v_{i,j+1} & v_{i+1,j+1} \end{bmatrix} \begin{bmatrix} 1 - y/b \\ y/b \end{bmatrix}$$

where

a = the size of the grid in the x direction,
b = the size of the grid in the y direction, and
x,y = element local coordinates with origin at the point (i,j).

There are many other shape functions discussed in the literature (see, for example, Strang *et al.* (1973), Zienkiewicz (1977), Schultz (1973)). Examples of such functions are the biquadratic and the ordinary bicubic function which are of class C^o, the hermitian bicubic function which is of class C^1, and the spline functions whose class depends on the degree of the spline used.

Lagrange's interpolation formula can also be used in two-dimensional interpolation. But this formula is more suitable for deriving theoretical results than for practical computations (Dahlquist, 1974).

A FINITE ELEMENT APPROACH FOR THE ANALYTICAL SELF-CALIBRATION METHOD

One of the basic systematic errors in photogrammetry is radial lens distortion. To compensate for this distortion, it can be assumed that each point on the image plane will have a different focal length.

The scale of the photograph is a function of the camera's focal length, and by assuming a different focal length for each image point, we are allowing a certain variation in the photo scale. This variation in the photo scale is also very effective in eliminating some of the image errors such as expansion or shrinkage of the photograph and the lack of flatness of the image surface.

TRIANGULAR ELEMENTS

The image plane domain can be divided into triangular element subdomains. By assuming that each point on the photograph will have a different focal length, the collinearity condition can be modified to the following form:

$$\begin{aligned} x_{ij} - x_{pi} &= f_{ij} (X'/Z')_{ij} \\ y_{ij} - y_{pi} &= f_{ij} (X'/Z')_{ij} \end{aligned} \qquad (6)$$

where

$$\begin{bmatrix} X' \\ Y' \\ Z' \end{bmatrix}_{ij} = \mathbf{M}_i \begin{bmatrix} X_j - X_i^c \\ Y_j - Y_i^c \\ Z_j - Z_i^c \end{bmatrix};$$

x_{pi}, y_{pi} = photographic coordinates of the principal point of the i^{th} photograph;
f_{ij} = focal length at the j^{th} point of the i^{th} photograph;
x_{ij}, y_{ij} = observed photo coordinates of point j on the i^{th} photograph;
X_j, Y_j, Z_j = object space coordinates of the j^{th} point;
X^C_i, Y^C_i, Z^C_i = object space coordinates of the i^{th} exposure station; and
$\mathbf{M}_i$ = unitary-orthogonal orientation matrix of the i^{th} photograph.

Let the symbol $\dot{\mathbf{u}}_i$ denote the exterior orientation parameters plus the principal point coordinates $(X^C Y^C, Z^C \omega, \phi, \kappa, x_p, y_p)$ of the i^{th} photograph, the

symbol $\ddot{\mathbf{u}}_i$ the focal length at point $j(f_{ij})$ of the i^{th} photograph, and the symbol $\dddot{\mathbf{u}}_j$ the object space coordinates (X,Y,Z) of the j^{th} point. Note that, in the above parameter vectors, there are no lens distortion coefficients as in other self-calibration methods. Equation 6 is linearized by Taylor's series expansion about the initial approximations for the unknown parameters. If all linearized equations are gathered, the collection of equations may be written in matrix notations as (ASP 1980)

$$\mathbf{V} + \dot{\mathbf{B}}\hat{\dot{\boldsymbol{\delta}}} + \ddot{\mathbf{B}}\hat{\ddot{\boldsymbol{\delta}}} + \dddot{\mathbf{B}}\hat{\dddot{\boldsymbol{\delta}}} = \boldsymbol{\epsilon} \tag{7}$$

where

$\dot{\boldsymbol{\delta}}$ = vector of corrections to the exterior orientation parameters and the principal point coordinates,

$\ddot{\boldsymbol{\delta}}$ = vector of correction to the focal lengths,

$\dddot{\boldsymbol{\delta}}$ = vector of corrections to the object space coordinates,

$\dot{\mathbf{B}}$ = matrix of partial derivatives of the collinearity equation with respect to the exterior orientation parameters and the principal point coordinates,

$\ddot{\mathbf{B}}$ = matrix of partial derivatives of the collinearity equation with respect to the focal lengths,

$\dddot{\mathbf{B}}$ = matrix of partial derivatives of the collinearity equation with respect to the object space coordinates,

$\mathbf{V}$ = residual vector for the image coordinates, and

$\boldsymbol{\epsilon}$ = discrepancy vector.

Treating all parameters as observed or pseudo-observed quantities of known *a priori* precision, the entire set of observation equations may be merged into a single observational equation system, giving rise to the following least-squares normal equations (Brown 1971):

$$\begin{bmatrix} \dot{\mathbf{B}}^T\mathbf{W}\dot{\mathbf{B}} + \dot{\mathbf{W}} & \dot{\mathbf{B}}^T\mathbf{W}\ddot{\mathbf{B}} & \dot{\mathbf{B}}^T\mathbf{W}\dddot{\mathbf{B}} \\ & \ddot{\mathbf{B}}^T\mathbf{W}\ddot{\mathbf{B}} + \ddot{\mathbf{W}} & \ddot{\mathbf{B}}^T\mathbf{W}\dddot{\mathbf{B}} \\ \text{SYM.} & & \dddot{\mathbf{B}}^T\mathbf{W}\dddot{\mathbf{B}} + \dddot{\mathbf{W}} \end{bmatrix} \begin{bmatrix} \hat{\dot{\boldsymbol{\delta}}} \\ \hat{\ddot{\boldsymbol{\delta}}} \\ \hat{\dddot{\boldsymbol{\delta}}} \end{bmatrix} = \begin{bmatrix} \dot{\mathbf{B}}^T\mathbf{W}\boldsymbol{\epsilon} - \dot{\mathbf{W}}\dot{\boldsymbol{\epsilon}} \\ \ddot{\mathbf{B}}^T\mathbf{W}\boldsymbol{\epsilon} - \ddot{\mathbf{W}}\ddot{\boldsymbol{\epsilon}} \\ \dddot{\mathbf{B}}^T\mathbf{W}\boldsymbol{\epsilon} - \dddot{\mathbf{W}}\dddot{\boldsymbol{\epsilon}} \end{bmatrix} \tag{8}$$

where $\mathbf{W}, \dot{\mathbf{W}}, \ddot{\mathbf{W}}, \dddot{\mathbf{W}}$ are, respectively, the weight matrices of the image coordinates, the elements of exterior orientation and the principal point coordinates, the focal length at each point, and the object space coordinates. The $\dot{\boldsymbol{\epsilon}}, \ddot{\boldsymbol{\epsilon}}, \dddot{\boldsymbol{\epsilon}}$ are vectors of residuals between the observed and current computed values. Equation 8 represents the general system of normal equations for the bundle adjustment of a photogrammetric block with finite element calibration.

RECTANGULAR ELEMENTS

In rectangular elements the focal length of a point inside an element can be expressed as a function of the focal length at the nodes of the rectangular element. With the above approach Equation 6 can be modified to the following form:

$$\begin{aligned} x_{ij} - x_{pi} &= g(f)\,(X'/Z')_{ij} \\ y_{ij} - y_{pi} &= g(f)\,(Y'/Z')_{ij} \end{aligned} \tag{9}$$

Using a bilinear function as in Equation 5,

$$g(f) = [1 - x/a,\ x/a] \begin{bmatrix} f_{i,j} & f_{i+1,j} \\ f_{i,j+1} & f_{i+1,j+1} \end{bmatrix} \begin{bmatrix} 1 - y/b \\ y/b \end{bmatrix}$$

where

$f_{i,j}$ = the focal length at node i,j; and

a,b = the dimension of the rectangular element in the x and y directions, respectively.

EXPERIMENTAL VERIFICATION OF THE FINITE ELEMENT APPROACH IN ANALYTICAL SELF-CALIBRATION

In order to verify the proposed finite element self-calibration technique and also to assess its practicability, an experiment was conducted (Munjy, 1982). The camera system used in the experiment consists of two MK-70 metric Hasselblad cameras, serial numbers 1146 and 1148, each with a Biogon 60-mm *f*/5.6 lens. The MK-70 incorporates a calibrated reseau plate with 25 crosses in a 1-cm by 1-cm grid pattern. The cameras were placed 0.60-m apart with their axes parallel to each other. The photographs were exposed using time of 1/2 second at *f*-stop 22. The two cameras were focused at 2 m. At *f*-stop 22 the depth of field was large enough so that all image points were in clear focus.

CONTROL FIELD

A three-dimensional object space control field was used. Veress and Tiwari (1976) and Fraser (1979) have given a complete description of the control field. This field consists of four piano wires suspended as plumb lines, each weighted with a heavy plumb bob immersed in an oil bath at one end and fixed to the ceiling by hooks at the other end. Small seed-beads of approximately 3-mm diameter are fixed on the wires to serve as target points. In all, 34 targets are available.

Precise theodolite surveys were carried out to determine the object space coordinates of the control points. A Zeiss TH2 theodolite was used to measure the horizontal and vertical angles to the target points

from the ends of a baseline, which was accurately measured by a steel tape lying flat on the floor.

The horizontal and vertical angles were transformed to pseudo-image coordinates and then a photogrammetric intersection program was used as suggested by Abdel Aziz (1975) to find the space coordinates of the control field points. The mean standard error of X, Y, Z coordinates in the control field was 0.155 mm.

IMAGE COORDINATE MEASUREMENTS

Image coordinates were observed on an OMI-Bendix AP/C. Each negative was observed monocularly. Besides observing the x,y coordinates for all target points, four reseau crosses were also observed, and an affine transformation was used to transform the machine coordinates to photo coordinates. In order to ensure rapid convergence of the camera calibration program, space resections were carried out so as to obtain reasonably refined preliminary estimates for the values of the exterior orientation elements at each camera station.

RESULTS AND ANALYSIS

Each Hasselblad camera lens system was calibrated individually by assuming that all object space coordinates of the points that were seen in each photograph were free from errors and by dividing the image plane into triangular elements. The calibration resulted in a focal length for each point as shown in Tables 1 and 2. The mean standard error of the focal length was 0.027 mm for camera 1146 and 0.033 mm for camera 1148.

The average principal point coordinate standard error was 0.015 mm. The root-mean-square (RMS) errors of the adjusted image coordinates were 0.0025 mm for camera system 1146 and 0.003 mm for camera system 1148.

By dividing the image plane for the Hasselblad camera into four rectangular elements, the focal length was represented by a bilinear function in each element. The focal length at each node, as shown in Table 3, was found by a least-squares adjustment. Points 10 and 11 on photo 1146 and 3 and 4 on photo 1148 had shown high residuals and they were dropped from the adjustment. The focal length

TABLE 1. HASSELBLAD 1146 FINITE ELEMENT CALIBRATION RESULTS

Point No.	Focal Length (mm)	Photo Coordinates x (mm)	Photo Coordinates y (mm)	Radial Distance r (mm)	Radial Lens Distortion r (mm)
3	63.378	23.965	3.809	23.990	0.012
8	63.403	0.299	10.356	10.329	0.009
10	63.224	0.371	− 4.298	4.326	−0.008
19	63.252	−15.839	9.723	18.806	−0.028
24	63.281	−15.727	−12.897	20.569	−0.022
29	63.442	24.085	−17.217	29.398	0.044
1	63.404	23.884	22.318	32.470	0.029
2	63.365	23.902	14.261	27.584	0.008
4	63.394	24.019	− 5.115	24.294	0.018
5	63.418	24.047	−12.539	26.889	0.030
6	63.340	0.245	22.309	22.282	−0.002
7	63.383	0.282	17.454	17.427	0.010
11	63.267	0.398	− 9.880	9.906	−0.013
18	63.224	−15.860	15.084	22.069	−0.043
20	63.258	−15.822	5.786	17.096	−0.024
21	63.250	−15.788	0.558	16.072	−0.024
22	63.268	−15.756	− 6.127	17.172	−0.022
23	63.275	−15.736	− 9.858	18.817	−0.021
25	63.303	−15.700	−16.939	23.303	−0.016
26	63.318	0.430	−15.051	15.079	−0.007
27	63.327	0.468	−20.803	20.831	−0.007
30	63.434	24.106	−20.700	31.584	0.043

Average focal length (f_o) = 63.347 mm

Mean standard error of the focal length = 0.027 mm

Principal point coordinates

x_p = 0.275 mm $\quad \sigma x_p$ = 0.012 mm

y_p = 0.027 mm $\quad \sigma y_p$ = 0.011 mm

The root mean square error of the adjusted image coordinates = 0.003 mm

[1] $r_i = [(x_i - x_p)^2 + (y_i - y_p)^2]^{1/2}$

[2] $r_i = r_i[(f_i/f_o) - 1]$

TABLE 2. HASSELBLAD 1148 FINITE ELEMENT CALIBRATION RESULTS

Point No.	Focal Length (mm)	Photo Coordinates x (mm)	Photo Coordinates y (mm)	Radial Distance r (mm)	Radial Lens Distortion r (mm)
3	63.335	0.029	2.817	2.681	0.003
8	63.284	−23.523	9.338	25.224	0.012
10	63.257	−23.497	− 5.287	24.079	0.001
9	63.272	−23.508	1.133	23.492	0.007
14	63.246	15.733	7.323	17.330	−0.002
33	63.231	15.930	−15.437	22.305	−0.008
29	63.212	0.154	−18.197	18.335	−0.012
1	63.352	− 0.063	21.187	21.050	0.033
2	63.334	− 0.045	13.204	13.067	0.017
4	63.168	0.097	− 6.086	6.224	−0.008
6	63.317	−23.535	21.224	31.572	0.031
11	63.257	−23.491	−10.898	25.920	0.001
12	63.244	15.690	13.933	20.921	−0.003
13	63.236	15.720	10.516	18.868	−0.005
15	63.246	15.790	1.932	15.929	−0.002
16	63.238	15.832	− 3.489	16.278	−0.004
17	63.250	15.877	− 7.569	17.682	−0.001
26	63.256	−23.484	−16.084	28.511	0.001
27	63.251	−23.464	−21.879	32.148	−0.002
30	63.165	0.171	−21.688	21.826	−0.031
32	63.222	15.898	−11.743	19.876	−0.010
34	63.222	15.957	−19.655	25.447	−0.013

Average focal length (f_o) = 63.254 mm

Mean standard error of the focal length = 0.033 mm
Principal point coordinates
x_p = −0.037 mm $\quad \sigma x_p$ = 0.017 mm
y_p = 0.037 $\quad \sigma y_p$ = 0.017 mm

The root mean square error of the adjusted image coordinates = 0.0025 mm

[1] $r_i = [(x_i - x_p)^2 + (y_i - y_p)^2]^{1/2}$
[2] $\delta r_i = r_i[(f_i/f_o) - 1]$

TABLE 3. HASSELBLAD MK-70 FOCAL LENGTH AT THE NODES OF THE RECTANGULAR FINITE ELEMENT CAMERA CALIBRATION

Node Number	Photo Coordinates x (mm)	Photo Coordinates y (mm)	Focal Length at the Nodes Camera 1146	Focal Length at the Nodes Camera 1148
1	−25.000	−25.000	63.333	63.255
2	0.000	−25.000	63.281	63.152
3	25.000	−25.000	63.466	63.252
4	−25.000	0.000	63.154	63.261
5	0.000	0.000	63.431	63.326
6	25.000	0.000	63.370	63.202
7	−25.000	25.000	63.149	63.324
8	0.000	25.000	63.344	63.352
9	25.000	25.000	63.396	63.165

TABLE 4. SPACE INTERSECTION RESULTS

Focal Length Representation	RMS (XYZ) of Object Space Points (mm)
Triangulaar Finite Element	0.160
Bilinear function in a square finite element	0.190

contour lines on the image plane for camera 1146 and 1148 are shown in Figures 3 and 4, respectively.

Computing the object space coordinates by intersection the, root-mean-square errors of the X,Y,Z coordinates listed in Table 4 were obtained.

CONCLUSION

The finite element calibration approach developed

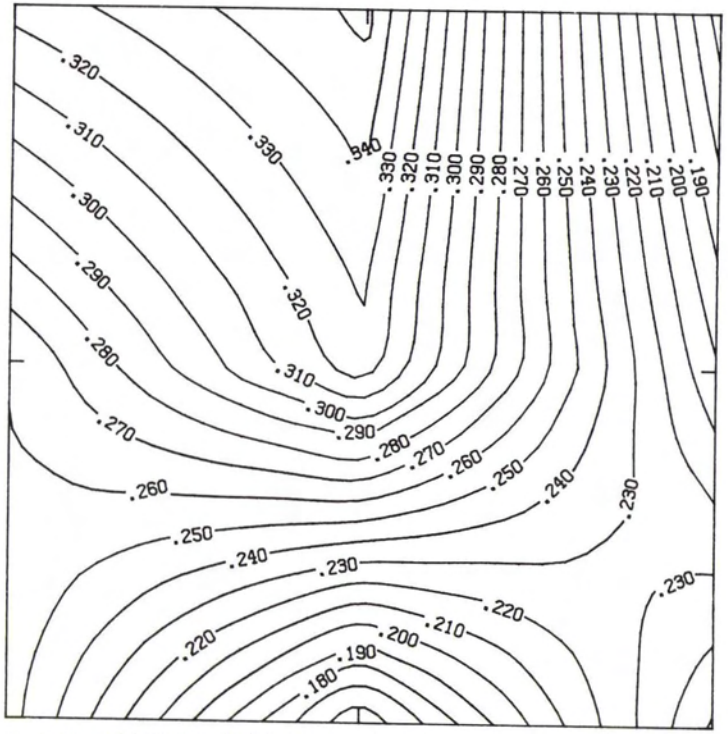

FIG.3. Hasselblad MK-70 (1146) focal length contour lines (initial focal length = 63.000 mm; contour interval = 0.010 mm; image size 25 mm by 25 mm).

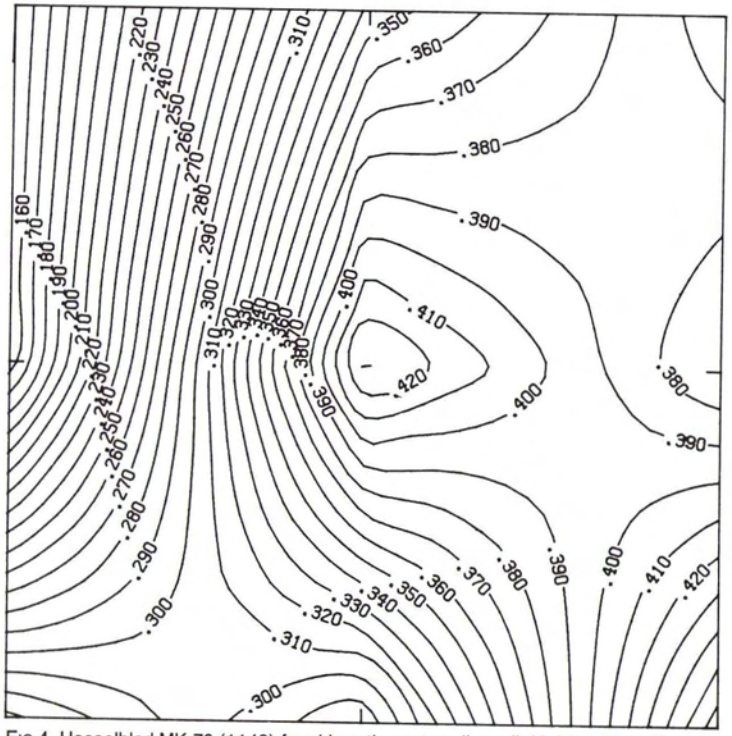

FIG.4. Hasselblad MK-70 (1148) focal length contour lines (initial focal length = 63.000 mm; contour interval = 0.010 mm; image size 25 mm by 25 mm).

in the previous sections has been employed for the calibration of two Hasselblad MK-70 metric cameras. Results obtained from the experimental verification of the finite element approach support the conclusion that this approach gives a good representation of systematic image errors in photogrammetry.

Due to the nature and the complexity of most systematic errors in photogrammetry, some difficulty will be encountered in representing these errors in mathematical models that would be valid throughout the image plane. This is especially true for film shrinkage, film flatness, and lens distortion. The use of these mathematical models to correct systematic errors can also introduce new errors that affect the precision of the photogrammetric results. In the finite element approach, we still have the same problem, but by dividing the image plane domain into subdomains or finite elements, a better representation of the systematic errors can be achieved.

Dividing the image plane into four rectangular elements and representing the focal length by a bilinear function gave results 15 percent worse than those for the triangular finite element approach. In spite of this difference between the accuracy of the triangular finite element approach and the rectangular finite element approach, the latter is recommended because there are fewer unknowns to be solved for in the observation equations. Also, if there are more points in the image domain, a finer rectangular mesh will give better results.

The attainment of higher accuracy in the finite element results for camera calibration depends very much on the accuracy of the image coordinate measurements. The so called first-order measuring instruments that are available on the market at present can measure image coordinates within an accuracy of about 0.001mm to 0.004mm. This measuring accuracy will permit us to assume the focal length as a variable quantity, and this forms the basis for the finite element approach in self-calibration.

In addition to self-calibration, the finite element method can be used in photogrammetric block adjustment to establish subsidiary control networks, and also for the correction of distortions in X-ray photogrammetry and satellite imagery.

Additional research still needs to be carried out on the use of more complicated trial functions in the elements, in order that higher accuracy may be achieved. Multiframe camera calibration with the finite element approach is worth development as well. The author believes that the use of the finite element technique in self-calibration is only the first of several possible applications of this technique that will contribute to the advancement of the state-of-the-art in analytical photogrammetry.

ACKNOWLEDGMENTS

The author expresses his gratitude to Professor S.A. Veress for his progressive guidance, valuable advice, and constant encouragement throughout the period of this research.

REFERENCES

Abdel-Aziz, Y. I., 1975. Construction of Three-Dimensional Control in Close Range Photogrammetry. *Proceedings of the 41st Annual Meeting of the American Society of Photogrammetry*, pp. 736–749.

American Society of Photogrammetry, 1980. *Manual of Photogrammetry*. 4th Edition.

Brown, D. C., 1971. Close-Range Camera Calibration. *Photogrammetric Engineering*, Vol. 37, No. 8, pp. 855–866.

———, 1972. Calibration of Close-Range Cameras. Press. Paper of Comm. III, XII Congress of ISP, Ottawa.

Cook, R. D., 1974. *Concepts and Applications of Finite Element Analysis*. John Wiley & Sons, Inc., New York, 402 p.

Dahlquist, G., 1974. *Numerical Methods*. Prentice Hall, Inc., Englewood Cliffs, New Jersey, 573 p.

Ebner, H., 1976. Self-Calibrating Block Adjustment, *Bul.*, 44,4, 128–139.

Ebner, H., and P. Reiss, 1978. Height Interpolation by the Method of Finite Elements. Presented Paper, ASP, Digital Terrain Symposium, St. Louis.

———, 1981. Experiences with Height Interpolation by Finite Elements. ASP-ACSM Fall Technical Meeting, San Francisco-Honolulu.

Ebner, H., B. Hofmann-Wellenhof, P. Reiss, and F. Steidler, 1980. HIFI — A Minicomputer Program Package for Height Interpolation by Finite Elements. Commission IV, ISP-Congress, Hamburg.

Ergatoudis, I., B. M. Irons, and O. C. Zienkiewicz, 1968. Curved, Isoparametric "Quadrilateral" Elements for Finite Element Analysis, *International Journal of Solids and Structures*, Vol. 4, No. 1, pp. 31–42.

Fraser, C. S., 1979. *Simultaneous Multiple Camera and Multiple Focal Setting Self-Calibration in Photogrammetry.*, Ph.D. Dissertation, University of Washington, Seattle, Washington.

Kenefick, J. F., M. S. Gyer, and B. F. Harp, 1972. Analytical Self-Calibration. *Photogrammetric Engineering*, Vol. 38, No. 11, pp. 1117–1126.

Munjy, R., 1982. *The Applications of The Finite Element Method in Photogrammetry*. Ph.D. Dissertation, University of Washington, Seattle, Washington.

Norrie, D. H., and G. DeVries, 1973. *The Finite Element Method*, Academic Press Inc., New York, 322 p.

Schultz, M. H., 1973. *Spline Analysis*, Prentice Hall Inc., Engelwood Cliffs, New Jersey, 156 p.

Strang, G., and G. J. Fix, 1973. *An analysis of the Finite Element Method*, Prentice Hall Inc., Englewood Cliffs, New Jersey, 306 p.

Veress, S. A., and R. S. Tiwari, 1976. Fixed Frame Multiple Camera System for Close Range Photogrammetry, *Photogrammetric Engineering and Remote Sensing*, Vol. 42, No. 9, pp. 1195–1210.

Zienkiewicz, O. C., 1977. *The Finite Element Method*, Third Edition, McGraw Hill Book Company Limited, London, United Kingdom, 787 p.

(Received 15 May 1985; accepted 31 July 1985; revised 15 October 1985)